RESEARCH ARTICLE

European Journal of **Soil Science** WILEY

Effects of longitudinal profile shape on scour and flow resistance in rills

Alessio Nicosia[1] 🔵 | **Vincenzo Palmeri**[1,2] | **Costanza Di Stefano**[1] | **Vincenzo Pampalone**[1] | **Gaetano Guida**[1] 🔵 | **Vito Ferro**[1,2] 🔵

[1]Department of Agricultural, Food and Forest Sciences, University of Palermo, Palermo, Italy

[2]NBFC, National Biodiversity Future Center, Palermo, Italy

Correspondence
Alessio Nicosia, Department of Agricultural, Food and Forest Sciences, University of Palermo, Viale delle Scienze, Building 4, 90128 Palermo, Italy.
Email: alessio.nicosia@unipa.it

Abstract

The literature regarding how rill longitudinal profile (concave and convex) affects soil loss and flow resistance is still lacking. The only analysis available in the literature for rills is limited by the fact that measurements were performed for a unique mean slope value s_p (18%). In this article, further rill measurements were conducted on a plot with $s_p = 15\%$ and complex profile shapes and were used to widen the knowledge about the influence of longitudinal profile shape on rill scour, eroded volume, and flow resistance. The findings highlighted that the concave profile has a homogeneous spatial distribution of moderate scours, whereas the scours in the convex one are deeper and more confined, but they are not placed after the slope change as found for $s_p = 18\%$. The mean scour depth, which accounts for the discharge and profile shape effects, is not (concave) or is weakly (convex) related to the flow discharge. The concave profile determined a reduction of approximately 57% of the total eroded volume when compared with the convex profile shape, confirming that a concave hillslope limits erosive phenomena. Finally, the flow resistance equation guaranteed a precise estimation of the Darcy–Weisbach friction factor.

KEYWORDS
concave profile, convex profile, longitudinal profile, rills, soil erosion

1 | INTRODUCTION

Despite being emphasized in several field studies, soil erosion is a significant environmental issue whose impacts are sometimes overlooked (Borrelli et al., 2017; Carollo et al., 2023; Di Stefano et al., 2023). An important step in understanding soil erosion phenomena is determining the relationship between hillslope characteristics and soil erosion processes. At the plot scale, the Universal Soil Loss Equation (USLE) (Wischmeier & Smith, 1978)

and its revised versions (e.g., RUSLE, USLE-MB) (Pampalone et al., 2023) highlight the relevance of the topographic factors (slope steepness and plot length) on the mean soil loss.

Uniform plots, i.e., characterized by a invariant slope steepness, have been used by many scholars to evaluate the influence of length and slope on soil erosion and runoff (Liu et al., 2023, 2024), but few investigations studied the impact of complex profile shapes as those concave or convex (Liu et al., 1994; Rieke-Zapp & Nearing, 2005).

The importance of the link between slope and profile shape was firstly underlined by Young and Mutchler (1969), who performed experiments at the plot scale, and obtained that concave hillslopes generally minimize sediment loss in comparison with uniform profiles. This result was then confirmed by different studies (Hancock et al., 2003; Jeldes et al., 2015; Rieke-Zapp & Nearing, 2005; Sensoy & Kara, 2014; Williams & Nicks, 1988) reported below. Five slope shape arrangements were implemented in the laboratory tests by Rieke-Zapp and Nearing (2005), who observed that soil loss for concave slopes was reduced by 75% in comparison with uniform ones that had the same surface area. Sensoy and Kara (2014) conducted experimental research in 9 field plots having distinct profile shapes that were set up on a 30% hillslope and exposed to natural rainfalls. According to their results, the maximum runoff and soil loss are obtained for the uniform slope, whereas the lowest values are obtained for the concave one. According to Jeldes et al. (2015), concave slopes imply a reduction from 15% to 40% in sediment loss when compared with the uniform ones. These decreased values are lower than those documented in the literature, which range from 50% (Williams & Nicks, 1988) to 80% (Hancock et al., 2003).

The only study reporting different findings was carried out by Mombini et al. (2021), using several complex hillslopes in laboratory experiments using three distinct soil surface roughness values and a unique rainfall intensity. The results showed that uniform parallel hillslopes exhibit the greatest reduction in soil loss because of increased soil roughness.

Rill erosion determines significant soil loss values at the hillslope scale (Bagarello & Ferro, 2010; Zhang et al., 2016) and is predominant in comparison with interrill erosion (Di Stefano et al., 2013). Moreover, nowadays, innovative methodologies to represent in detail the hillslope surface (Javernick et al., 2014) are available. Nevertheless, the scientific community has barely looked into the rill erosion phenomena for complex profiles. The erosion phenomena occurring in rills are affected by flow hydraulics (Govers et al., 2007) and, therefore, the study of flow resistance becomes an important step in understanding and modelling erosion processes (Di Stefano et al., 2022a).

To the best of our knowledge, rill flow resistance for complex hillslopes was only studied by Nicosia, Di Stefano, et al. (2022). They performed experimental runs on a plot set with concave, convex, and uniform profiles and a mean slope $s_p = 18\%$, evaluated how longitudinal profile shape affects the flow resistance law, scour depth, and eroded volume. These authors assessed, for plots having complex morphologies, the applicability of a theoretical approach, developed for flows moving in rills shaped on uniform plots (Di Stefano et al., 2022a), to

Highlights

- The concave profile has a homogeneous spatial distribution of moderate scours.
- The scours in the convex profile are deeper and more confined.
- The concave profile determined a reduction of approximately 57% of the total eroded volume.

deduce the Darcy–Weisbach friction factor f (Ferro, 2018). The results by Nicosia, Di Stefano, et al. (2022) demonstrated that the flow resistance law guarantees a reliable estimate of f for each profile shape. The f rate resulting from the shape in a convex profile was found to be between 3.4 and 26.9% of the overall friction factor, whereas in a concave profile, it ranged from 0.68 to 14.6%. According to the authors' findings, the scour was equally distributed for the uniform and concave profiles, whereas it was prevalently located downstream of the slope change for the convex profile. Nicosia, Di Stefano, et al. (2022) demonstrated that the scour depth measured at the rill thalweg SD and its mean value SD_m generally increase with discharge. Moreover, the ratio SD/SD_m may be assumed to be independent of discharge for both concave and convex profile shapes. Finally, the authors found a reduction in total eroded rill volume of 57.9% for the concave profile compared with the uniform one.

However, the analysis by Nicosia, Di Stefano, et al. (2022) was developed using measurements performed for a unique mean slope value. For this reason, in this study, the investigation of the influence of the longitudinal profile shapes (concave and convex) on scour depth, eroded volume, and flow resistance equation was extended, including measurements obtained for a mean s_p value of 15% in the perspective to overcome the knowledge gap concerning the slope effect. In detail, the main objectives of this investigation are to (i) compare the differences determined by the change of the mean plot slope, evaluating the scour and the eroded volumes obtained for flows characterized by comparable discharges for the analysed profile shapes and (ii) test the reliability of the theoretical approach by Ferro (2018).

2 | MATERIALS AND METHODS

2.1 | The experimental setup and measurement techniques

The experimental runs were conducted on a 2 m (width) × 7 m (length) plot (Figure 1) situated in the

experimental area of the Department of Agriculture, Food and Forest Sciences (AFFS) of the University of Palermo. Concave and convex profile shapes were set, preparing the plot (Figure 1a,b) dividing it into two 3.27-m long parts having two slopes (12 and 18%), obtaining a mean plot slope s_p equal to 15% (Figure 1c). For both profile shapes, the soil was the clay loam used by Nicosia, Di Stefano, et al. (2022) (36.4% sand, 30.9% silt, and 32.7% clay), and the preliminary operations were conducted following their same methodologies to assure the comparability of the investigated conditions (cohesion, soil bulk density, soil moisture, shaping phase). The soil used to fill the experimental plot was collected in the area surrounding the Department AFFS (38° 06′ 25″ N, 13° 20′ 59″ E). This area is characterized by a typical Mediterranean climate (*Csa*, according to the Köppen classification; Köppen, 1918) and vegetation. The soil was collected from different points within the area to consider field variation. The abovementioned soil texture was determined by the hydrometer method for fine size fractions and mechanical dry sieving for coarse fractions, applied to five samples homogeneously distributed on the plot surface. Another five soil samples were collected by steel cylinders of known dimensions (5 cm in height and 5 cm in diameter) to determine bulk density (1.23 g cm^{-3}), by oven-drying at

105°C for 24 h. The organic matter content of the soil, determined by oven-drying the samples in a muffle furnace at 400°C, is approximately equal to 2%. To ensure a homogeneous soil moisture, before starting the experiments, the plot soil was wetted until ponding condition. Each rill was manually incised following the maximum slope direction of the plot, and then shaped by a clear flow discharge Q (0.1 L s^{-1}) applied for 3 min. This procedure was applied to ensure that the shaped rills (i.e., artificial) are comparable to naturally formed rills. Overall, eight rills were shaped for the concave profile shape and four for the convex one. After the shaping phase ($Q = 0.1$ L s^{-1}) and before the beginning of each experimental run with a specific flow discharge, each rill showed the same longitudinal profile shape of the plot and was divided into nine segments, delimited by two cross-sections located at a distance of 0.624 m. For the experiments, a constant clear inflow discharge Q was applied. In particular, for the concave profile, $Q = 0.23, 0.29, 0.33, 0.39, 0.46, 0.49, 0.56,$ and 0.64 L s^{-1} were tested, whereas for the convex one, $Q = 0.28, 0.38, 0.48,$ and 0.65 L s^{-1} were applied.

A series of 70 photos and Agisoft Photoscan Professional were used to build the 3D-DTM of the plot area. The slope gradient of each rill segment was determined by the thalweg identified by the 3D-DTM. By averaging
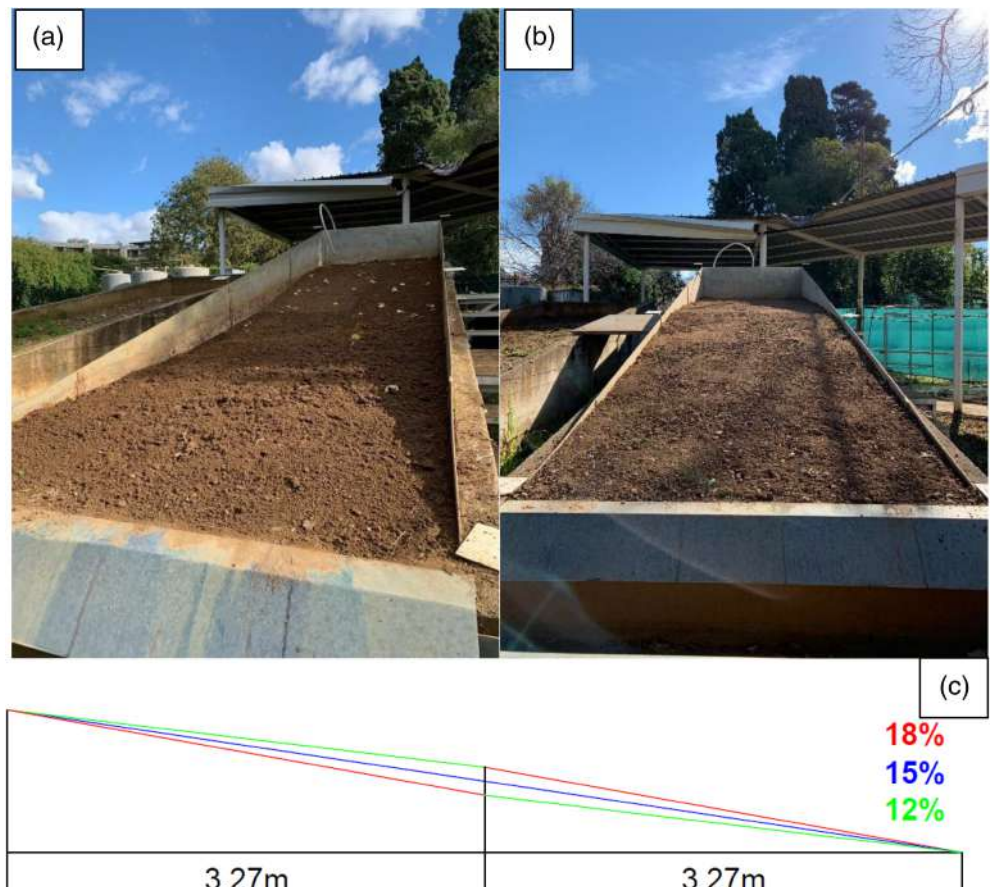

FIGURE 1 Experimental plot with concave (a), and convex (b) profile shape, and scheme of the investigated concave and convex profile shapes (c).

the data collected in the reach under consideration, the slope s of each reach was determined.

Applying the technique presented by Di Stefano et al. (2019), the mean water depth h and hydraulic radius R of each reach were estimated. By using close-range photogrammetry, this technique combines a precise rill survey with that of the water tracks inside it, identified by a dye. The h and R values were calculated, starting from the measured flow depths and geometric cross-sections given by the 3D-DTM with a 6.2 cm interdistance within the reach, applying the following relationships (Di Stefano et al., 2019):

$$h = \frac{\sum_{i=2}^{N-1}\left(\frac{\sigma_1}{2} + \sigma_i + \frac{\sigma_N}{2}\right)}{\sum_{i=2}^{N-1}\left(\frac{w_1}{2} + w_i + \frac{w_N}{2}\right)} \quad (1)$$

$$R = \frac{\sum_{i=2}^{N-1}\left(\frac{\sigma_1}{2} + \sigma_i + \frac{\sigma_N}{2}\right)}{\sum_{i=2}^{N-1}\left(\frac{C_1}{2} + C_i + \frac{C_N}{2}\right)} \quad (2)$$

in which σ and C are, respectively, the hydraulic cross-section area and the wetted perimeter in the reach, w is the surface width, and N is the cross-section number in the reach.

To detect flow velocity, a Methylene blue solution was used as a dye tracer (Di Stefano et al., 2020; Nicosia et al., 2021). A correction factor of 0.8 was used to adjust the measured surface velocity to the mean flow velocity V (Di Stefano et al., 2021; Zhang et al., 2010).

The measurements gave Reynolds numbers $\mathrm{Re} = Vh/\nu_k$, where ν_k is the water kinematic viscosity, corresponding to turbulent flows ($2752 \leq \mathrm{Re} \leq 10{,}630$ for the concave profile (72 runs) and $6167 \leq \mathrm{Re} \leq 13{,}640$ for the convex one (36 runs)) and Froude numbers $F = V/\sqrt{gh}$, where g is the gravitational acceleration, corresponding to subcritical and supercritical flows ($0.65 \leq F \leq 2.26$ for the concave profile and $0.47 \leq F \leq 1.83$ for the convex one).

The frequency distributions of F, f, s, and V for both the examined profiles are shown in Figure 2.

For a set of runs (4 rills) for both profile shapes, the Digital Elevation Models (DEMs) after the rill shaping phase (D1) and after the conclusion of the experiments (D2) were used to determine the corresponding longitudinal profiles of the rill thalweg, which were used to determine the scour depth values SD (i.e., the differences in height between the longitudinal profile for D1 and D2). For each rill, the mean scour depth SD_m was obtained by averaging the SD values. The DEMs were also used for calculating the pixel elevation differences between D2 and D1 by the DEM of difference (DoD). The total eroded rill volume RV was calculated by the DoD. The DEMs are characterized by a minimum level of detection of ± 0.003 m. Consequently, variations in bed elevation in the range of ± 0.003 m cannot be detected.

2.2 | The rill flow resistance equation

Under the hypothesis of Incomplete Self-Similarity (ISS) in $u_* y / \nu_k$ (Barenblatt & Monin, 1979; Butera et al., 1993) (where $u_* = (g\,R\,s)^{0.5}$ is the shear velocity, and y is the distance from the bottom) neglecting the influence of Re (turbulent flow regime) and considering that the flow Froude number also considers the ratio h/d (Ferro, 2018) (where d is the median soil particle diameter), the integration of the dimensionless functional relationship, representing the local flow velocity profile $v(y)$ along a certain vertical for an open-channel flow (Barenblatt, 1987, 1993; Ferro, 1997), leads to:

$$\frac{v}{u_*} = \Gamma(s, F)\left(\frac{u_* y}{\nu_k}\right)^{\delta} \quad (3)$$

where $\Gamma(s, F)$ is a function to be defined by velocity measurements and δ can be obtained as (Castaing et al., 1990):

$$\delta = \frac{1.5}{\ln \mathrm{Re}} \quad (4)$$

The following expression of f is deduced (Barenblatt, 1993; Ferro & Porto, 2018) by integrating Equation (3):

$$f = 8\left[\frac{2^{1-\delta}\,\Gamma\,\mathrm{Re}^{\delta}}{(\delta+1)(\delta+2)}\right]^{-2/(1+\delta)} \quad (5)$$

By setting equal to $\alpha\,h$ the distance y at which the local velocity is equal to the cross-section average velocity V, the following estimate Γ_v of Γ function (Ferro & Porto, 2018) is obtained from the velocity profile (Equation 3):

$$\Gamma_v = \frac{V}{u_*\left(\frac{u_*\,\alpha\,h}{\nu_k}\right)^{\delta}} \quad (6)$$

The coefficient α, which is less than 1, considers that both V is located below the water surface and the mean

FIGURE 2 Empirical frequency distributions of F (a), f (b), s (c), and V (d).
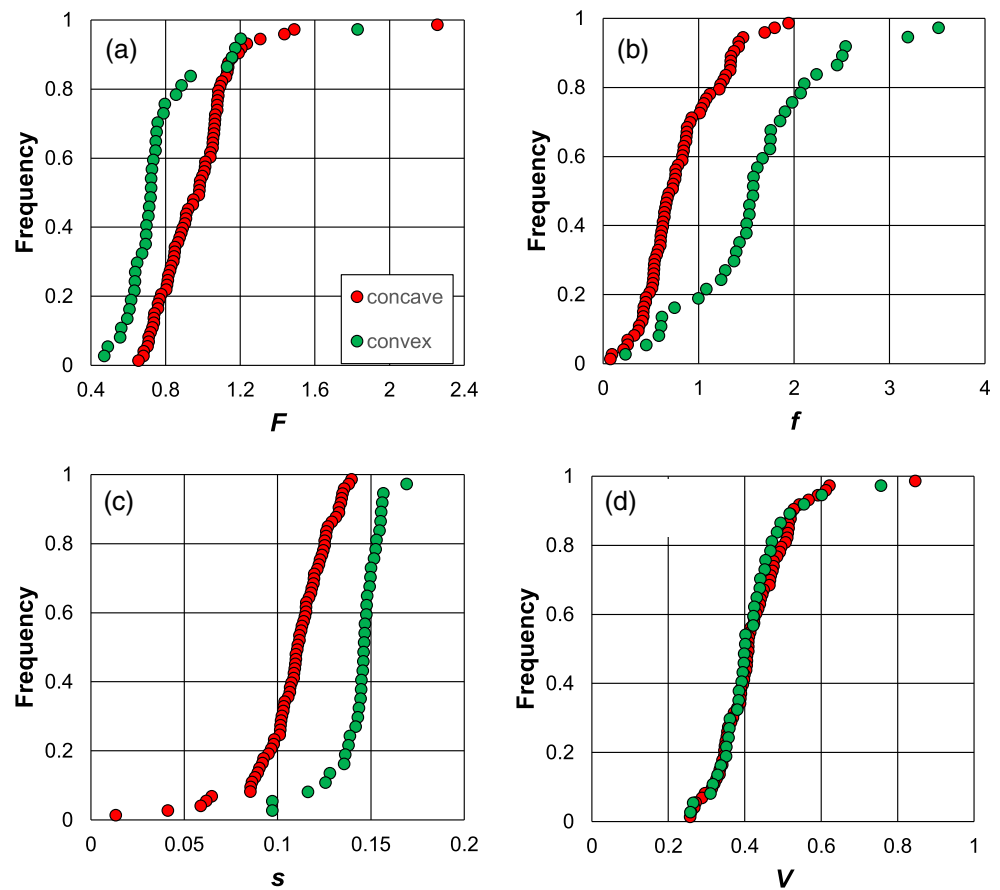
velocity profile in the cross-section is considered. For this study, α had low variability and the mean value (0.124) was used.

Ferro (2018) demonstrated that Γ theoretically depends only on s and F following this power equation:

$$\Gamma_v = a\,\frac{F^b}{s^c} \qquad (7)$$

where a, b, and c are coefficients derived from experimental data.

3 | RESULTS

3.1 | Soil erosion in concave and convex plots

As an example, for single rills for concave (Figure 3a,b) and convex (Figure 3c,d) profile shapes, Figure 3 plots the rill longitudinal profiles at the end of the shaping phase (D1) and at the end of the experiments (D2), for mean plot slopes s_p of 15 (this investigation) and 18% (Nicosia, Di Stefano, et al., 2022).

For each profile shape, the frequency distribution of the SD/SD_m ratio corresponding to the four investigated discharges (ranging from 0.29 to 0.56 L s^{-1} for the concave profile (Figure 4a) and from 0.28 to 0.65 L s^{-1} for the convex one (Figure 4b)) is shown in Figure 4. The latter demonstrates that, also in this case, SD/SD_m can be assumed independent of discharge for both the profile shapes. Figure 4c shows, as an example for a single discharge value ($\approx$0.47 L s^{-1}), the empirical frequency distribution of SD/SD_m for each profile shape. The overlapping of the two distributions suggests that SD/SD_m is not dependent on profile shape.

The measurements performed in this study show an absent (concave) or weak (convex) relationship between SD_m and Q for each profile shape, and that the mean scour depths for convex profile are higher than those for the concave profile (Figure 5).

The DoDs for the concave (a) and convex (b) profiles, characterized by a similar range of Q (0.29–0.56 L s^{-1} for the concave profile shapes and 0.28–0.65 L s^{-1} for the convex one), are shown in Figure 6. This figure also shows the DoDs for the concave (Figure 6c) and convex (Figure 6d) profile shapes obtained by Nicosia, Di Stefano, et al. (2022) for $s_p = 18\%$.
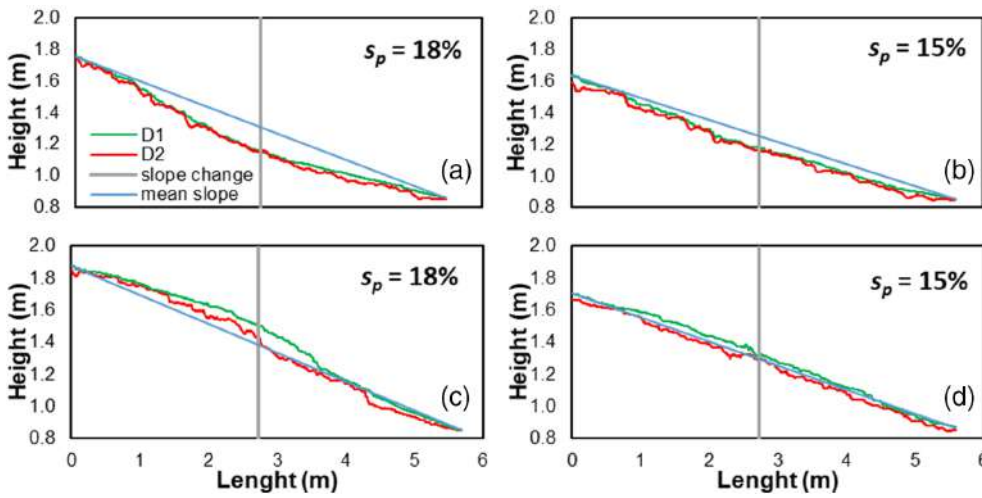
FIGURE 3 Examples of rill longitudinal profiles at the end of the shaping phase (D1) and at the end of the experimental runs (D2), for mean plot slopes s_p of 15 (this investigation) (b and d) and 18% (a and c) (Nicosia, Di Stefano, et al., 2022).

The DoD obtained for both profile shapes allowed for calculating the total eroded *volume RV* of each rill. The comparison between the flow discharge Q and RV is shown in Figure 7 as an example for four rills analysed for each profile shape. This figure shows that, except for the run with $Q = 0.46$ L s^{-1} of the concave profiles, as expected, RV increases with Q. The sum of the *four RV values* was equal to 0.0393 m^3 for the concave profile and 0.0915 m^3 for the convex one.

3.2 | Analysis of the Darcy-Weisbach friction factor for concave and convex profile shapes

The 108 (72 for the concave and 36 for the convex profile) measurements performed in this study were added to the 143 (71 for the concave and 72 for the convex profile) measurements by Nicosia, Di Stefano, et al. (2022), to calibrate Equation (7), including all the available data and neglecting the effect of the profile shape, obtaining:

$$\Gamma_v = 0.4064 \frac{F^{1.08}}{s^{0.5464}} \qquad (8)$$

characterized by a coefficient of determination R^2 equal to 0.996. Coupling Equations (8) and (5), the following flow resistance equation is obtained:

$$f = 8 \left[\frac{(\delta+1)(\delta+2)}{2^{1-\delta} Re^\delta \, 0.4064} \frac{s^{0.5464}}{F^{1.08}} \right]^{2/(1+\delta)} \qquad (9)$$

The estimate of f given by Equation (9) has a good agreement, characterized by a root mean square error RMSE

equal to 0.121, between the measured Darcy–Weisbach friction factor values and those calculated by Equation (9) (Figure 8a). The f values calculated by Equation (9) are characterized by errors always $\leq\pm20\%$ and $\leq\pm10\%$ for 94% of cases. Figure 8a also shows that, averagely, the f values for the convex profile are higher than those obtained for the concave one.

To study the differences determined by the profile shape on flow resistance, the theoretical flow resistance law was calibrated for both the concave and convex profile shapes, obtaining:

$$\Gamma_v = 0.4065 \frac{F^{1.0962}}{s^{0.5475}} \qquad \text{(concave)} \qquad (10a)$$

$$\Gamma_v = 0.4328 \frac{F^{1.0652}}{s^{0.5044}} \qquad \text{(convex)} \qquad (10b)$$

characterized by R^2 of 0.993 and 0.992, respectively. Coupling Equation (10a,b) and (5), the following flow resistance equation is obtained:

$$f = 8 \left[\frac{(\delta+1)(\delta+2)}{2^{1-\delta} Re^\delta \, 0.4065} \frac{s^{0.5475}}{F^{1.0962}} \right]^{2/(1+\delta)} \qquad \text{(concave)}$$

$$(11a)$$

$$f = 8 \left[\frac{(\delta+1)(\delta+2)}{2^{1-\delta} Re^\delta \, 0.4328} \frac{s^{0.5044}}{F^{1.0652}} \right]^{2/(1+\delta)} \qquad \text{(convex)} \quad (11b)$$

The agreement between the measured f values and those calculated by Equation (11a,b), characterized by a RMSE equal to 0.112, is plot in Figure 8b. The f values calculated by Equation (11a,b) are characterized by errors always $\leq\pm20\%$ and $\leq\pm10\%$ for 93.6% of cases.
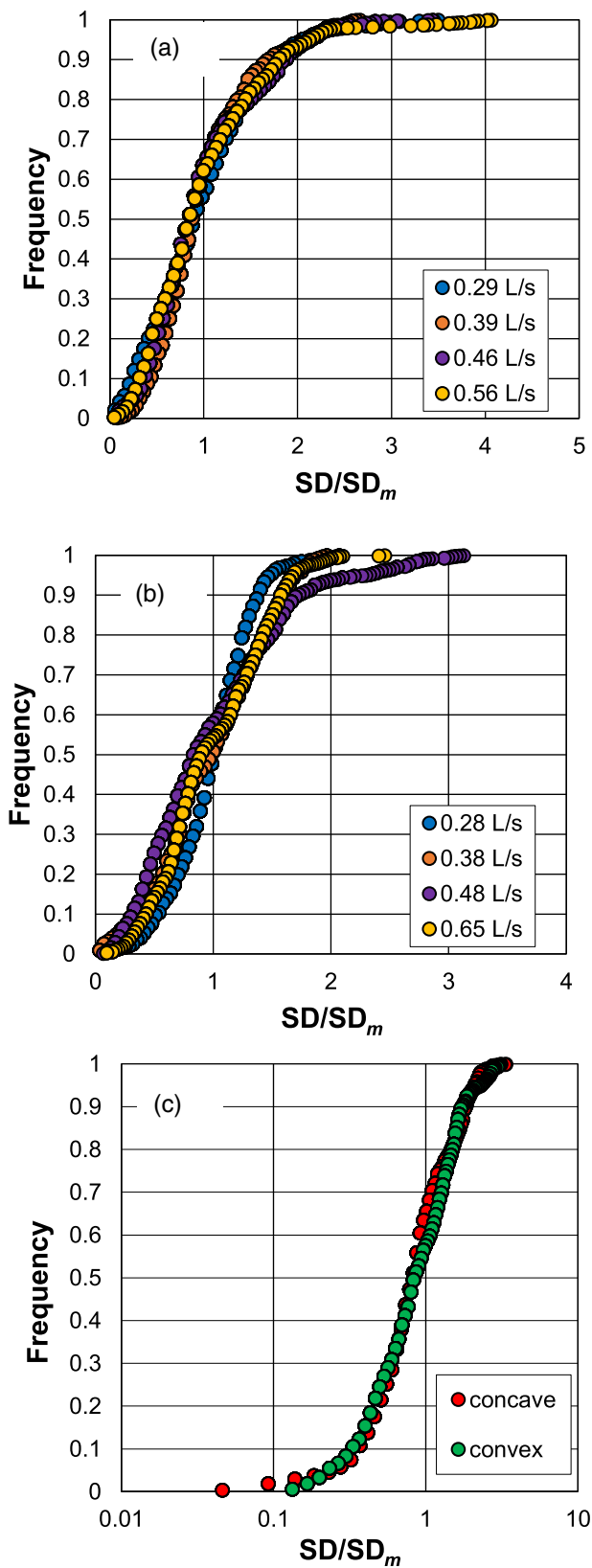
FIGURE 5 Relationship between the investigated discharge values and the SD_m for both profile shapes.

FIGURE 4 Frequency distribution of the SD/SD_m ratio corresponding to the four investigated discharges for the concave (a) and the convex (b) profiles, and as an example for a single discharge value (≈0.47 L s^{-1}), of the ratio SD/SD_m for each profile shape (c).
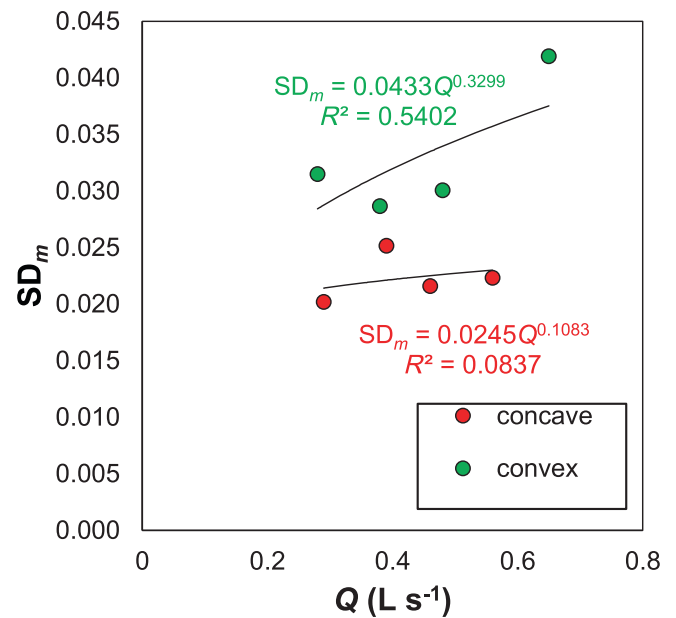
4 | DISCUSSION

4.1 | Soil erosion in concave and convex plots

For both the investigated mean plot slopes, the concave profile shape is characterized by a homogeneous spatial distribution of moderate scours, whereas the convex one has more localized and deeper scours (Figures 3 and 6). For the convex profile, Nicosia, Di Stefano, et al. (2022) found that the scour was mostly located after the slope change justifying this result as a transition from a gentle (GS) (12%) to a steep (SS) (24%) slope. In fact, previous investigations (Nicosia, Palmeri, et al., 2022; Peng et al., 2015) suggested a slope threshold of 18% to distinguish between the GS and SS, highlighted by differences in hydraulic (h, V, Re, F) and sediment transport (flow transport capacity T_c, actual sediment load) variables. In particular, Nicosia, Palmeri, et al. (2022) concluded that T_c for the SS is not a limiting factor for the sediment transport, whereas both T_c and the soil particle detachability and transportability limit the actual sediment transport for the GS. In other words, Nicosia, Di Stefano, et al. (2022) found a concentrated scour downstream of the slope change as, in this half of the rill, the sediment transport was not limited by T_c, differently from the upstream half. Instead, the result of this investigation (Figures 3d and 6) highlights that the convex profile is characterized by localized scours uniformly distributed along the rill and less relevant than those detected by Nicosia, Di Stefano, et al. (2022). This result could be
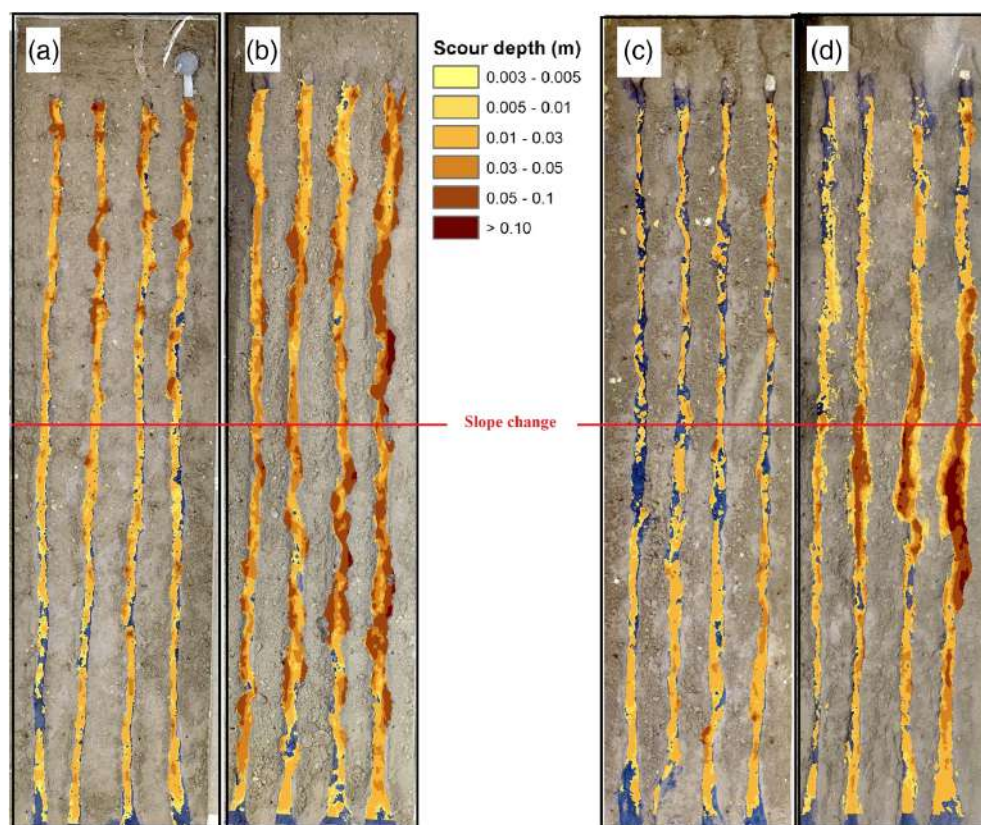
FIGURE 6 DoDs obtained for the concave (a) and convex (b) profile shapes in this study and DoDs for the concave (c) and convex (d) profile shapes obtained by Nicosia, Di Stefano, et al. (2022) for $s_p = 18\%$.
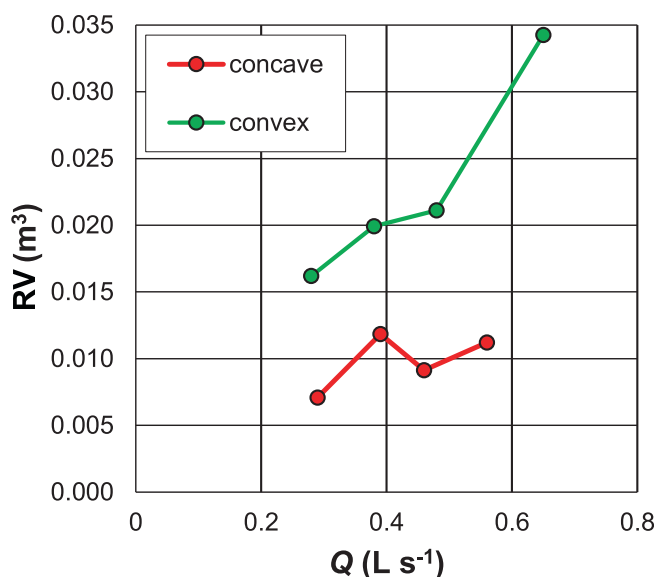

FIGURE 7 Comparison, as an example for four rills analysed for each profile shape, between the applied discharge Q and total eroded volume RV.

condition. In other words, the actual sediment transport is limited by the sediment transport capacity also downstream of the slope change. Moreover, the applied inflow discharges determined scour phenomena but did not change the convex and concave profile shapes, as testified by the fact that the rill longitudinal profile shape remained basically the same before and after the experimental runs (Figure 3).

The outcome by Nicosia, Di Stefano, et al. (2022) that SD/SD_m can be assumed independent of discharge and profile shape was confirmed (Figure 4). So, the SD_m accounts for the discharge and profile shape effects regardless of the investigated mean plot slope.

The mean scour depth SD_m is not related to flow discharge for the concave profile shape and is weakly related to it for the convex one (Figure 5). This result does not agree with that presented by Nicosia, Di Stefano, et al. (2022), who found that the mean scour depth increases with discharge following a power relationship dependent on the profile shape.

In agreement with the studies by Di Stefano et al. (2022b) and Nicosia, Di Stefano, et al. (2022), the eroded volumes generally increase with Q (Figure 7). The finding that SD_m is weakly or not related to Q, while the eroded volume is, can be explained by the circumstance that the DoD considers the spatial distribution of scour depth, whereas the mean scour depth represents the mean value
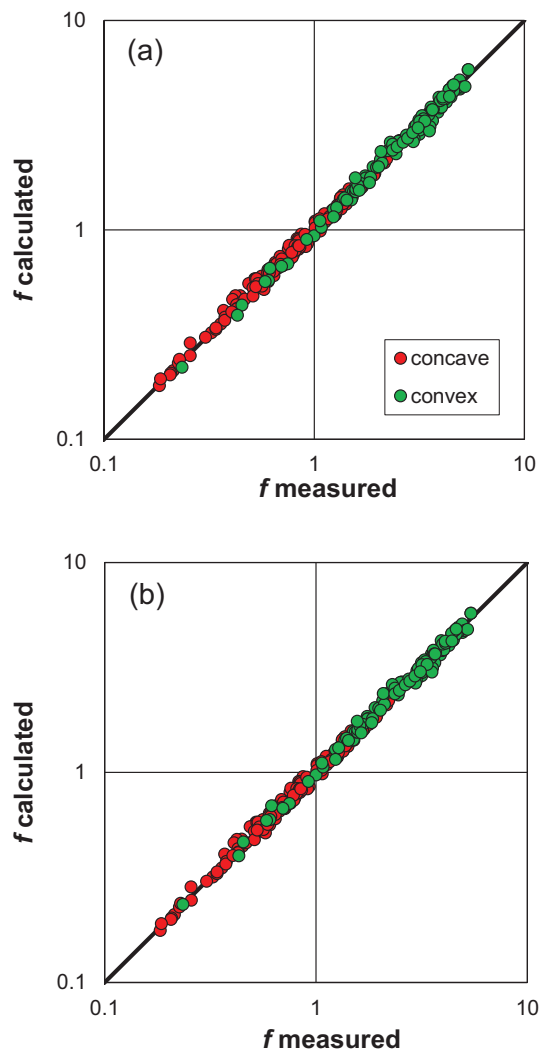
explained by the circumstance that the convex profile investigated here is characterized by a slope of 18% downstream of the slope change, which represents the threshold between GS and SS, and consequently, the entire rill can be considered to be characterized by a gentle slope

FIGURE 8 Comparison between the 251 measured Darcy–Weisbach friction factor values and those calculated by Equation (9) (a) and by Equation (11a,b) (b).

of measurements along a unique linear flow path. In other words, especially for the concave profile shape, for the highest values of flow discharge, the eroded volumes correspond to rills that are wider and less deep than those shaped by the lowest discharges.

Finally, the sum of the four RV values highlights that the concave profile determines a reduction of approximately 57% of soil loss when compared with the convex profile shape, as already obtained by Nicosia, Di Stefano, et al. (2022). Many authors (Hancock et al., 2003; Jeldes et al., 2015; Liu et al., 1994) found that concave hillslopes yield soil loss reductions ranging from 50% to 80% when compared with uniform and convex ones. Therefore, this study confirms that the rill erosive phenomena in a concave profile are limited.

In conclusion, the present investigation highlights that the change of mean plot slope in comparison with Nicosia, Di Stefano, et al. (2022) yielded (i) a different

distribution of eroded volumes along the rill path for the convex profile, and (ii) the relation between mean scour depth and flow discharge is not significant.

4.2 | Analysis of the Darcy-Weisbach friction factor for concave and convex profile shapes

The investigated flows for both profile shapes have tendentially overlapped ranges of Reynolds number. The convex profile has F values lower than those of the concave profile, and $F < 1$ for 86% of cases. These results confirm that the profile shape determines differences in the kinematic flow variables but not in the flow regime, as already found for $s_p = 18\%$ (Nicosia, Di Stefano, et al., 2022).

The patterns of the hydraulic and geometric variables are tendentially the same as those obtained by Nicosia, Di Stefano, et al. (2022) (Figure 2). The Froude number values of the concave plot are higher than those of the convex one (Figure 2a), whereas the Darcy–Weisbach and s values of the concave profile are lower than those of the convex profile (Figure 2b,c). Instead, the two profile shapes feature comparable values of flow velocity (Figure 2d), differently from Nicosia, Di Stefano, et al. (2022), who obtained lower V values for the convex profile. Even if differences in terms of flow velocity occur, as found by Nicosia, Di Stefano, et al. (2022), the highest RV (Figure 7) for the convex profile point out more relevant erosive processes producing an increase in grain roughness and sediment transport, and consequently f (Figure 2b).

The theoretical approach guarantees a reliable estimate of f (Figure 8). In detail, despite the differences in hydraulic characteristics at the reach scale, a unique flow resistance law (Equation 9) can be applied to the two profile shapes.

Since, in this study, a unique soil has been investigated, the applicability of Equations (9) and (11a,b) should be tested for other soils, characterized by different physicochemical characteristics (e.g., texture, aggregation, cohesion). The assessment of the applicability of these equations to other experimental conditions would represent a huge step in water and soil conservation studies, as the Darcy-Weisbach friction factor is commonly used to estimate flow velocity in process-oriented soil erosion models.

5 | CONCLUSIONS

The developed analysis confirmed that the concave profile shape is characterized by a uniform spatial distribution of moderate scours, whereas the convex one has more localized and deeper scours. However, in this study, the convex profile is not characterized by a scour

localized after the slope change, as found in the literature, but the localized scours are uniformly distributed along the rill. Moreover, the mean scour depth determined at the rill thalweg, accounting for the influence of the discharge and profile shape, is not related to the flow discharge for the concave profile shape and is weakly related to it for the convex one. The concave profile determined a reduction of approximately 57% of the overall eroded volume when compared with the convex profile shape, confirming that a concave hillslope limits erosive phenomena. The results also demonstrated that the profile shape affects the kinematic flow variables, while it does not influence the flow regime. Finally, the equation to estimate Γ was calibrated using all the available data and a reliable estimate of f was attained. The approach accuracy is only marginally improved by calibrating Γ on data from a specific profile shape.

AUTHOR CONTRIBUTIONS

Alessio Nicosia: Conceptualization; investigation; writing – original draft; methodology; validation; writing – review and editing; formal analysis; data curation; software. **Vincenzo Palmeri:** Conceptualization; investigation; methodology; validation; writing – review and editing; formal analysis; data curation; writing – original draft; software. **Costanza Di Stefano:** Conceptualization; investigation; writing – original draft; methodology; validation; writing – review and editing; formal analysis; data curation; supervision; software. **Vincenzo Pampalone:** Conceptualization; investigation; writing – original draft; methodology; validation; writing – review and editing; formal analysis; software; data curation. **Gaetano Guida:** Conceptualization; investigation; writing – original draft; methodology; validation; writing – review and editing; software; formal analysis; data curation. **Vito Ferro:** Supervision; data curation; formal analysis; software; methodology; validation; writing – review and editing; writing – original draft; investigation; conceptualization.

ACKNOWLEDGEMENTS

DATA AVAILABILITY STATEMENT

The data that support the findings of this study are available from the corresponding author upon reasonable request.

ORCID

Alessio Nicosia https://orcid.org/0000-0003-0540-8788
Gaetano Guida https://orcid.org/0000-0002-7718-4392
Vito Ferro https://orcid.org/0000-0003-3020-3119

REFERENCES

Bagarello, V., & Ferro, V. (2010). Analysis of soil loss data from plots of different length for the Sparacia experimental area, Sicily, Italy. *Byosystems Engineering*, *105*, 411–422.

Barenblatt, G. I. (1987). *Dimensional analysis*. Science Publishers Inc.

Barenblatt, G. I. (1993). Scaling laws for fully developed turbulent shear flows, part 1, Basic hypothesis and analysis. *Journal of Fluid Mechanics*, *248*, 513–520.

Barenblatt, G. I., & Monin, A. S. (1979). Similarity laws for turbulent stratified flows. *Archive for Rational Mechanics and Analysis*, *70*, 307–317.

Borrelli, P., Robinson, D. A., Fleischer, L. R., Lugato, E., Ballabio, C., Alewell, C., Meusburger, K., Modugno, S., Schütt, B., Ferro, V., Bagarello, V., Van Oost, K., Montanarella, L., & Panagos, P. (2017). An assessment of the global impact of 21st century land use change on soil erosion. *Nature Communications*, *8*(1), 1–13.

Butera, L., Ridolfi, L., & Sordo, S. (1993). On the hypothesis of self-similarity for the velocity distribution in turbulent flows. *Excerpta*, *8*, 63–94.

Carollo, F. G., Di Stefano, C., Nicosia, A., Palmeri, V., Pampalone, V., & Ferro, V. (2023). A new strategy to assure compliance with soil loss tolerance at a regional scale. *Catena*, *223*, 106945.

Castaing, B., Gagne, Y., & Hopfinger, E. J. (1990). Velocity probability density functions of high Reynolds number turbulence. *Physica D*, *46*, 177–200.

Di Stefano, C., Ferro, V., Pampalone, V., & Sanzone, F. (2013). Field investigation of rill and ephemeral gully erosion in the Sparacia experimental area, South Italy. *Catena*, *101*, 226–234.

Di Stefano, C., Nicosia, A., Palmeri, V., Pampalone, V., & Ferro, V. (2020). Dye-tracer technique for rill flows by velocity profile measurements. *Catena*, *185*, 104313.

Di Stefano, C., Nicosia, A., Palmeri, V., Pampalone, V., & Ferro, V. (2021). Flume experiments for assessing the dye-tracing technique in rill flows. *Flow Measurement and Instrumentation*, *77*, 101870. https://doi.org/10.1016/j.flowmeasinst.2020.101870

Di Stefano, C., Nicosia, A., Palmeri, V., Pampalone, V., & Ferro, V. (2022a). Rill flow velocity and resistance law: A review. *Earth Science Reviews*, *231*, 104092. https://doi.org/10.1016/j.earscirev.2022.104092

Di Stefano, C., Nicosia, A., Palmeri, V., Pampalone, V., & Ferro, V. (2022b). Rill flow resistance law under sediment transport. *Journal of Soils and Sediments*, *22*, 334–347. https://doi.org/10.1007/s11368-021-03083-x

Di Stefano, C., Nicosia, A., Pampalone, V., & Ferro, V. (2023). Soil loss tolerance in the context of the European Green Deal. *Heliyon*, *9*(1), e12869.

Di Stefano, C., Nicosia, A., Pampalone, V., Palmeri, V., & Ferro, V. (2019). New technique for measuring water depth in rill channels. *Catena*, *181*, 104090. https://doi.org/10.1016/j.catena.2019.104090

Ferro, V. (1997). Applying hypothesis of self-similarity for flow-resistance law of small-diameter plastic pipes. *Journal of Irrigation and Drainage Engineering*, *123*, 175–179.

Ferro, V. (2018). Assessing flow resistance in gravel bed channels by dimensional analysis and self-similarity. *Catena*, *169*, 119–127. https://doi.org/10.1016/j.catena.2018.05.034

Ferro, V., & Porto, P. (2018). Applying hypothesis of self-similarity for flow resistance law in Calabrian gravel bed rivers (Fiumare). *Journal of Hydraulic Engineering*, *144*, 1–11.

Govers, G., Giménez, R., & Van Oost, K. (2007). Rill erosion: Exploring the relationship between experiments, modelling and field observations. *Earth Science Reviews*, *84*(3–4), 87–102.

Hancock, G. R., Loch, R. J., & Willgoose, G. R. (2003). The design of post-mining landscapes using geomorphic principles. *Earth Surface Processes and Landforms*, *28*(10), 1097–1110.

Javernick, L., Brasington, J., & Caruso, B. (2014). Modeling the topography of shallow braided rivers using structure-from-motion photogrammetry. *Geomorphology*, *213*, 166–182.

Jeldes, I. A., Drumm, E. C., & Yoder, D. C. (2015). Design of stable concave slopes for reduced sediment delivery. *Journal of Geotechnical and Geoenvironmental Engineering*, *141*(2), 04014093. https://doi.org/10.1061/(ASCE)GT.1943-5606.0001211

Köppen, W. (1918). Classification of climates according to temperature, precipitation and seasonal cycle. *Petermanns Geographische Mitteilungen*, *64*(1918), 193–203.

Liu, B. Y., Nearing, M. A., & Risse, L. M. (1994). Slope gradient effects on soil loss for steep slopes. *Transactions of the American Society of Agri-Cultural Engineers*, *37*(6), 1835–1840. https://doi.org/10.13031/2013.28273

Liu, Y., Liu, G., Xiao, H., Dan, C., Shu, C., Han, Y., Zhang, Q., Guo, Z., & Zhang, Y. (2023). Predicting the interrill erosion rate on hillslopes incorporating soil aggregate stability on the Loess Plateau of China. *Journal of Hydrology*, *622*, 129698. https://doi.org/10.1016/j.jhydrol.2023.129698

Liu, Y., Liu, G., Xiao, H., Xia, X., Zhang, Q., Zhou, Z., Li, H., Zheng, F., Guo, Z., & Liu, D. (2024). Sediment sorting and transport mechanism controlled by both soil properties and hydraulic parameters on hillslopes. *Journal of Hydrology*, *634*, 131069. https://doi.org/10.1016/j.jhydrol.2024.131069

Mombini, A., Amanian, N., Talebi, A., Kiani-Harchegani, M., & Rodrigo-Comino, J. (2021). Surface roughness effects on soil loss rate in complex hillslopes under laboratory conditions. *Catena*, *206*, 105503. https://doi.org/10.1016/j.catena.2021.105503

Nicosia, A., Di Stefano, C., Palmeri, V., Pampalone, V., & Ferro, V. (2021). Roughness effect on the correction factor of surface velocity for rill flows. *Hydrological Processes*, *35*(10), e14407. https://doi.org/10.1002/hyp.14407

Nicosia, A., Di Stefano, C., Palmeri, V., Pampalone, V., & Ferro, V. (2022). Evaluating the effects of the rill longitudinal profile on flow resistance law. *Water*, *14*, 326. https://doi.org/10.3390/w14030326

Nicosia, A., Palmeri, V., Pampalone, V., Di Stefano, C., & Ferro, V. (2022). Slope threshold in rill flow resistance. *Catena*, *208*, 105789.

Pampalone, V., Nicosia, A., Palmeri, V., Serio, M. A., & Ferro, V. (2023). Rill and interrill soil loss estimations using the USLE-MB equation at the Sparacia experimental site (South Italy). *Water*, *15*(13), 2396.

Peng, W., Zhang, Z., & Zhang, K. (2015). Hydrodynamic characteristics of rill flow on steep slopes. *Hydrological Processes*, *29*(17), 3677–3686.

Rieke-Zapp, D., & Nearing, M. A. (2005). Slope shape effects on erosion: A laboratory study. *Soil Science Society of America Journal*, *69*(5), 1463–1471. https://doi.org/10.2136/sssaj2005.0015

Sensoy, H., & Kara, O. (2014). Slope shape effect on runoff and soil erosion under natural rainfall conditions. *iForest*, *7*, 110–114.

Williams, R. D., & Nicks, A. D. (1988). Using CREAMS to simulate filter strip effectiveness in erosion control. *Journal of Soil and Water Conservation*, *43*(1), 108–112.

Wischmeier, W. H., & Smith, D. D. (1978). *Predicting rainfall erosion losses: A guide to conservation planning*. USDA agriculture handbook No 537, U.S. Department of Agriculture, Washington, DC, USA.

Young, R. A., & Mutchler, C. K. (1969). Effect of slope shape on erosion and runoff. *Transactions of the American Society of Agri-Cultural Engineers*, *12*, 231–233.

Zhang, G., Luo, R., Cao, Y., Shen, R., & Zhang, X. C. (2010). Correction factor to dye-measured flow velocity under varying water and sediment discharges. *Journal of Hydrology*, *389*, 205–213.

Zhang, P., Tang, H., Yao, W., Zhang, N., & Xizhi, L. V. (2016). Experimental investigation of morphological characteristics of rill evolution on loess slope. *Catena*, *137*, 536–544.